Symmetry replication and toroidic effects in the multiferroic pyroxene $NaFeSi_2O_6$

Bruno Mettout,[1] Pierre Tolédano,[1] and Manfred Fiebig[2]
[1]*Laboratory of Physics of Complex Systems, University of Picardie, 33 rue Saint-Leu, 80000 Amiens, France*
[2]*HISKP, Universität Bonn, Nussallee 14-16, 53115 Bonn, Germany*
(Received 7 April 2010; revised manuscript received 12 May 2010; published 11 June 2010)

The magnetoelectric and toroidic effects occurring in $NaFeSi_2O_6$ are analyzed theoretically. The symmetry-breaking mechanism giving rise to the incommensurate antiferromagnetic-ferroelectric phase observed below 6 K is shown to be induced by replication of a single transition order parameter. It implies an effective-continuous symmetry of the system identified as the phason rotation of the incommensurate order parameter. The magnetic-field induced toroidal moment is expressed in terms of the macroscopic and spin variables. It shows that the toroidal susceptibility components vary critically as the electric polarization, denoting the inherently magnetoelectric nature of the scaling properties of the ferrotoroidic state. The toroidal moment arising under applied field in antiferromagnetic-ferroelectric structures is induced simultaneously with a spin wave which exhibits the same symmetry properties but spans different degrees of freedom. The difference between microscopic spins degrees of freedom and the electromagnetic macroscopic magnetization and toroidal fields is emphasized.

DOI: 10.1103/PhysRevB.81.214417 PACS number(s): 77.80.−e, 61.50.Ah, 75.80.+q

I. INTRODUCTION

The resurgence of interest in magnetoelectric multiferroic materials has prompted discussion of the relevance of the concept of magnetic toroidal moment for clarifying the macroscopic and microscopic properties of these systems.[1–4] The existence in antiferromagnetic structures of a macroscopic moment asymmetric under both time reversal and space inversion long remained elusive[5–7] until the recent observation by optical second harmonic generation of the independent coexistence of ferrotoroidic and antiferromagnetic domains in the weak-ferromagnetic structure of $LiCoPO_4$.[8] This result provides a motivation for investigating toroidic effects in the ferroelectric phases of magnetic multiferroic materials, in which the space-asymmetric electric polarization is induced by a time-asymmetric and space-asymmetric antiferromagnetic order. Here we describe theoretically the magnetoelectric and toroidic effects in the pyroxene compound $NaFeSi_2O_6$ (NFS). We show that the antiferromagnetic-ferroelectric phase observed below 6 K (Ref. 9) results from the coupling of two order-parameters *displaying the same symmetry*. This *symmetry replication* of the primary order parameter, which is permitted by the invariance of the free energy under the continuous rotation of the phase modulation mode (phason) associated with the incommensurate spin wave, is unique among the presently known multiferroic compounds, such as $TbMnO_3$,[10] $MnWO_4$,[11] or $Ni_3V_2O_8$,[12] in which the electric polarization is induced by the coupling of antiferromagnetic order-parameters having different symmetries.[13–15] The magnetic-field-induced toroidal moment $\vec{T}$ in NFS is expressed in function of the macroscopic order-parameters and microscopic spins. The field-induced toroidal moment appears simultaneously with a spin wave displaying the same symmetry properties, but spanning different degrees of freedom. The toroidal susceptibility components are shown to exhibit the same critical behavior as the electric polarization.

The paper is organized as follows: in Sec. II we recall the concept of symmetry replication that was introduced in the theoretical description of systems displaying a *continuous* broken symmetry[16–18] and explain why it can also apply to the incommensurate ferroelectric phase of magnetic multiferroic materials in which *discrete* symmetries are broken. This is illustrated in Sec. III by the theoretical analysis of the magnetoelectric properties observed in NFS.[9] The toroidic properties of NFS are then described at the macroscopic (Sec. IV A) and microscopic (Sec. IV B) levels.

II. SYMMETRY REPLICATION IN INCOMMENSURATE MULTIFERROICS

One of the distinctive feature of most of the presently known magnetic multiferroic materials is the existence of a sequence of two second-order transitions to antiferromagnetic incommensurate phases, in which the first more symmetric (nonpolar) phase is induced by a single irreducible representation (IR) Γ_1 of the parent paramagnetic phase associated with the incommensurate $\vec{k}$ vector, whereas the second less-symmetric ferroelectric phase is generated by the coupling $(\Gamma_1+\Gamma_2)$ of two distinct IR's of the parent phase corresponding to the same $\vec{k}$ vector. Combining *once* Γ_1 with Γ_2 can give rise to a number of less symmetric phases that should exhaust the list of possible magnetic phases that may appear in the material in presence or absence of applied magnetic field. This result is valid when the symmetry group broken at the transition is *discrete*. However, we have shown within the contexts of superconductivity[16] and liquid crystals[17,18] that the polymorphism of the low-symmetry phases extends beyond the conventional phases induced by a *single copy* of Γ_1 and Γ_2 when the broken symmetry is *continuous*. It relates to the property that the *lowest*-symmetry group induced by the IR Γ_1 of a continuous symmetry group G_0 can only be obtained by considering the *reducible* representation $\Gamma_1+\Gamma_1+\Gamma_1+\cdots$. The number n of Γ_1 figuring in the sum can be calculated on using group-theoretical methods described in Ref. 18. It is always smaller or equal to the dimension N of Γ_1, i.e., $\Gamma_1+\Gamma_1$ for $N=2$. This result stems

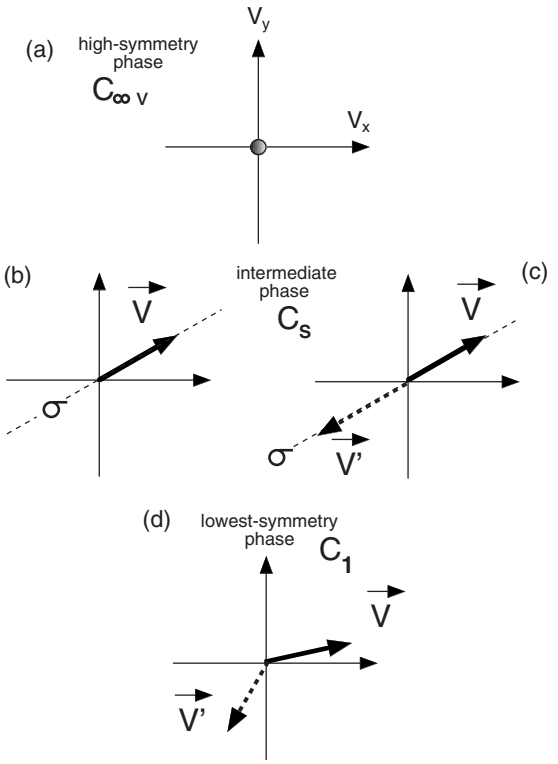

FIG. 1. Symmetry replication mechanism. (a) In the parent high-symmetry phase, the vector order parameter vanishes, and the continuous symmetry group is $\infty.m$ ($C_{\infty v}$). When only one vector order parameter (b) or two collinear order parameters (c) are involved, a single ordered phase is stabilized which possesses the symmetry m generated by the reflexion σ. By contrast, two dephased noncollinear order parameters (d) stabilize an additional vector state having the lowest-symmetry group 1, reduced to the identity.

from the group-theoretical rule that the *minimal symmetry group* G_m induced by Γ_1, defined as the invariance group of the general direction in the representation space, does not coincide with the *lowest-symmetry group* G_k associated with Γ_1, corresponding to the kernel of the homomorphism of G_0 on $\Gamma_1(G_0)$. Therefore, in order to obtain the full set of broken-symmetry phases associated with Γ_1 one has to consider the coupling of *n copies* of Γ_1. This specific property of continuous groups is illustrated by a simple example in Fig. 1: the IR Γ_1 of a parent phase, with continuous rotational (isotropic) symmetry, induces an anisotropic phase showing a polar vector $\vec{V}$ invariant by a mirror plane symmetry σ, which forms with the identity 1 the minimal symmetry group G_m associated with Γ_1. Considering an additional noncollinear vector $\vec{V}'$ induced by Γ_1, and invariant by a different mirror plane σ', yields stabilization of the lowest-symmetry group $G_k=1$ associated with $\Gamma_1+\Gamma_1$, which leaves invariant $\vec{V}$ and $\vec{V}'$.

The preceding mechanism of *symmetry replication* of the order parameter does not apply to structural or magnetic transitions giving rise to strictly periodic structures, since they involve discrete symmetry-breaking mechanisms. By contrast, if the order parameter is associated with structural or magnetic waves with incommensurate wave vectors it is well known[19] that the thermodynamic features of the transition to the incommensurate phase are driven by an *effective continuous group* generated by the images of the incommensurate crystallographic translations in the order-parameter space: the discrete translation group which is broken at the transition to the incommensurate (structural or magnetic) structure has a *dense* image in the order-parameter space *acting as the continuous rotation group of the phason*. Consequently, unconventional low-symmetry phases induced by several copies of the same IR can be stabilized at incommensurate structural or magnetic transitions as the result of a continuous symmetry-breaking mechanism. In the following section we show that this is indeed the case for the incommensurate ferroelectric phase observed below 6 K in NFS.

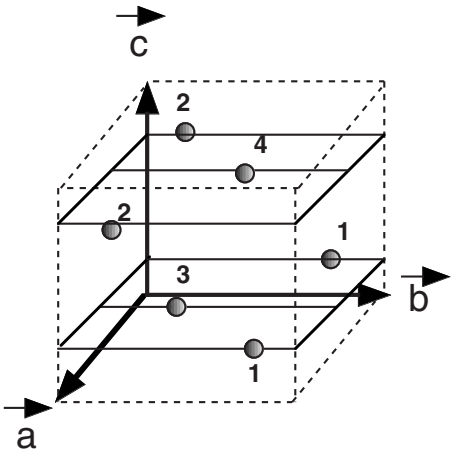

FIG. 2. Position of the Fe atoms in the conventional monoclinic unit-cell of the paramagnetic structure of NFS. Atoms 1, 2, 3 and 4 are located, respectively, at $(0,1-\delta,1/4)$, $(0,\delta,3/4)$, (1/2,1/2-$(1/2,1/2-\delta,1/4)$, and $(1/2,1/2+\delta,3/4)$.

III. MAGNETOELECTRIC PROPERTIES OF NFS

A. Symmetry replication in NSF

Below its paramagnetic phase of magnetic symmetry C2/c1′ (Fig. 2) NFS undergoes at $T_N=8$ K and $T_F=6$ K second-order phase transitions associated with the incommensurate wave vector $\vec{k}=(0,0.77,0)$.[20] The high-temperature ordered phase is incommensurate and paraelectric, whereas the low-temperature phase is ferroelectric. A third magnetic phase is stabilized at low temperature under applied magnetic field. Two irreducible representations (IR's) of $C2/c1'$, denoted Γ^+ and Γ^- (Table I), can give rise to magnetic transitions in the $\vec{k}$ direction of the monoclinic-C Brillouin zone. Two sets of physical quantities (continuous magnetic waves and localized spins) can be used for a concrete interpretation of the corresponding order parameters. A first natural set is provided by magnetic waves freezing at the transitions. Thus, Γ^+ is spanned by a single antiparallel longitudinal magnetic wave, expressed by the magnetic moment,

$$\vec{m}^b(y) = (\eta_b e^{iky} + \eta_b^* e^{-iky})\vec{b}, \tag{1}$$

where the amplitudes η_b and η_b^* are the order-parameter components, and $\vec{b}$ is the basic lattice vector along the two-

TABLE I. Generators of the irreducible representations Γ^+ and Γ^- of the $C2/c1'$ paramagnetic space groups for $\vec{k}=(0,k,0)$. C_2 is the twofold rotation axis along $\vec{b}$, I the space inversion, T the time-reversal and $\vec{t}=(0,b,0)$. $\varepsilon=e^{ik.\vec{t}}$.

$C2/c1'$	$\left(C_2\middle\vert 00\frac{c}{2}\right)$	$(\mathrm{I}\vert 000)$	T	$\vec{t}$
Γ^+	$\begin{pmatrix}1 & \\ & 1\end{pmatrix}$	$\begin{pmatrix}1 & \\ & 1\end{pmatrix}$	$\begin{pmatrix}-1 & \\ & -1\end{pmatrix}$	$\begin{pmatrix}\varepsilon & \\ & \varepsilon*\end{pmatrix}$
Γ^-	$\begin{pmatrix}-1 & \\ & -1\end{pmatrix}$	$\begin{pmatrix}1 & \\ & 1\end{pmatrix}$	$\begin{pmatrix}-1 & \\ & -1\end{pmatrix}$	$\begin{pmatrix}\varepsilon & \\ & \varepsilon*\end{pmatrix}$

fold axis. Γ^- is associated with two transversely polarized magnetic waves,

$$\vec{m}^a(y) = (\eta_a e^{iky} + \eta_a^* e^{-iky})\vec{a},$$

$$\vec{m}^c(y) = (\eta_c e^{iky} + \eta_c^* e^{-iky})\vec{c}, \tag{2}$$

where both order parameters (η_a, η_a^*) and (η_c, η_c^*) transform as Γ^-. Considering first a single copy of each representation Γ^+ and Γ^- yields the Landau expansion,

$$F_1 = a_1\rho_1^2 + a_2\rho_2^2 + \frac{b_1}{2}\rho_1^4 + \frac{b_2}{2}\rho_2^4 + a_3\rho_1^2\rho_2^2\cos 2\varphi + \frac{a_4}{2}\rho_1^4\rho_2^4\cos^2 2\varphi, \tag{3}$$

with $\eta_b=\rho_1 e^{i\varphi_1}$, $\eta_b^*=\rho_1 e^{-i\varphi_1}$, $\eta_a(\text{or } \eta_c)=\rho_2 e^{i\varphi_2}$, $\eta_a^*(\text{or } \eta_c^*)=\rho_2 e^{-i\varphi_2}$, and $\phi=\phi_1-\phi_2$. Figure 3 shows the phase diagram resulting from the minimization of F_1. It contains five possible stable phases labeled I-to-V. Figure 4 summarizes the equilibrium conditions fulfilled by each phase and their magnetic point-groups. One can unambiguously identify phase II, induced by Γ^-, as corresponding to the antiferromagnetic phase reported in NFS below T_N, since its magnetic structure, with the point-group $2/m1'$, exhibits collinear Fe-spins oriented in the $\vec{a}$-$\vec{c}$ plane, as observed experimentally.

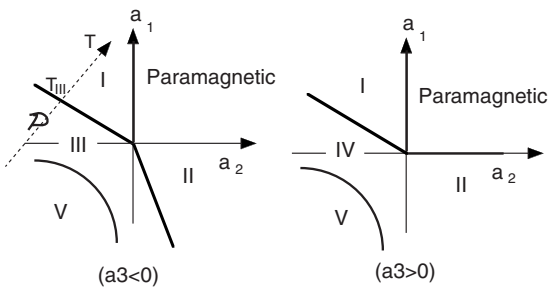

FIG. 3. Phase diagrams associated with the free energy F_1 [Eq. (3)] for (a) $a_3<0$ and (b) $a_3>0$. All curves correspond to second-order transitions. Phases II and III are respectively observed in NFS below T_N and above a threshold magnetic field B_{th}.

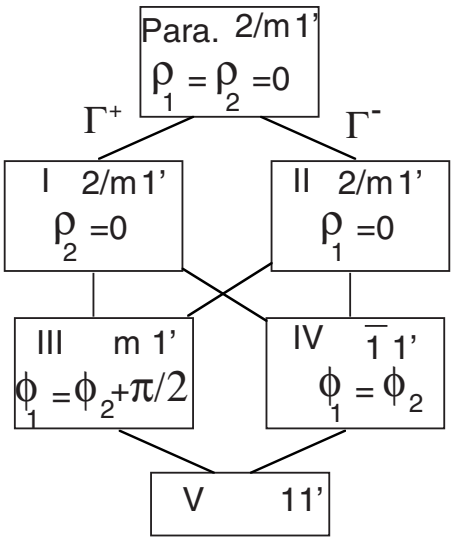

FIG. 4. Connection between the magnetic point groups of phases I-to-V, obtained by minimization of F_1, and equilibrium conditions fulfilled by the coupled order-parameter for each phase.

Figure 4 shows that none of the polar phases III and V induced by $\Gamma^+ + \Gamma^-$ coincide with the ferroelectric phase with P^b polarization reported in NFS below T_F. Let us show that the stabilization of this latter phase results from *the coupling of the two transversally polarized magnetic waves* $\vec{m}^a(y)$ and $\vec{m}^c(y)$. Such a coupling stabilizes an additional broken-symmetry phase under the condition that *the two waves correspond to different phases* φ_2 and φ_2' of the order parameter, i.e., $\eta_a=\rho_2 e^{i\varphi_2}$ and $\eta_c=\rho_2' e^{i\varphi_2'}$, with $\varphi_2-\varphi_2' \neq (0,\pi)$. The corresponding Landau expansion,

$$F_2 = a_2\rho_2^2 + a_2'\rho_2'^2 + 2a_3\rho_2\rho_2'\cos(\varphi_2-\varphi_2') + \frac{b_2}{2}\rho_2^4 + \frac{b_2'}{2}\rho_2'^4 + b_3\rho_2^2\rho_2'^2\cos^2(\varphi_2-\varphi_2') \tag{4}$$

yields the phase diagram shown in Fig. 5. It contains, below the range of stability of phase II, an additional phase II′ of symmetry $2_b1'$, which exhibits an electric polarization P^b as

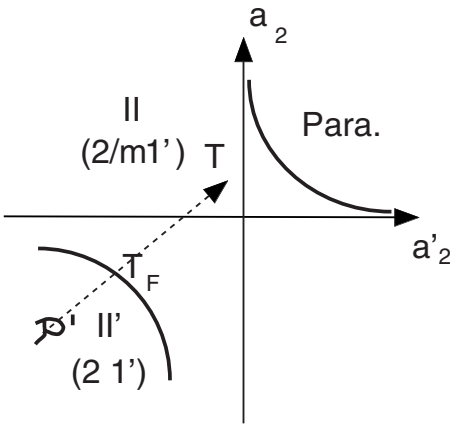

FIG. 5. Phase diagram associated with the free energy F_2 [Eq. (4)]. The curves correspond to second-order transitions. Phase II′ is observed below T_F in NFS.

observed below T_F in NFS. Accordingly, the low-temperature incommensurate phase observed in NFS results from the coupling of two order parameters having the same symmetry, i.e., transforming as the same IR Γ^- of the paramagnetic phase. As emphasized in Sec. II, this symmetry-replication mechanism, which is disclosed for the first time in a multiferroic compound, is allowed by the possibility of fixing arbitrarily the phase of the order parameter, due to the continuous rotation of the phase modulation mode. It therefore permits a coupling between *dephased* order parameters displaying the same symmetry.

Note that the coupling of two dephased longitudinal magnetic waves $\vec{m}^b$ [Eq. (1)] would lead to a similar sequence of phases $2/m1'$(phase I)$\rightarrow 2_b1'$(phase I$'$). However, in phases I and I$'$ the twofold rotation imposes Fe spins oriented along $\vec{b}$, whereas in phases II and II$'$ the twofold rotation combines with time reversal in a way that the Fe spins lie in the $\vec{a}$-$\vec{c}$ planes, as reported experimentally.[9]

B. Magnetoelectric behavior

Along the straight thermodynamic path $\mathcal{P}'$ shown in Fig. 5, the temperature dependences of a_2 and a_2' can be parameterized as: $a_2=a_{20}(T_F-T)+\sigma b_2 a_3/\sqrt{b_3}$ $a_2'=a_{20}'(T_2-T)+b_2'a_3/\sqrt{b_3}$, where a_{10}, a_{20} and σ are constants characterizing the path. The order-parameter amplitudes $\rho_2=(-a_2/b_2)^{1/2}$ and $\rho_2'=(-a_2'/b_2')^{1/2}$ *vary noncritically* at T_F, while the dephasing $\varphi_2-\varphi_2'$ *plays the role of the critical transition order parameter*. It varies below T_F as

$$\sin(\varphi_2-\varphi_2')\approx\left[\frac{\sqrt{b_3}}{a_3}\left(\frac{\sigma a_{20}'}{b_2'}+\frac{a_{20}}{\sigma b_2}\right)\right]^{1/2}\sqrt{T_F-T}. \quad (5)$$

Minimizing the dielectric free energy,

$$F_C=-\chi\vec{P}\,.\,\vec{E}-\alpha\rho_2\rho_2'P^b\sin(\varphi_2-\varphi_2')+\frac{\lambda_{aa}}{2}P^aP^a+\frac{\lambda_{bb}}{2}P^bP^b+\frac{\lambda_{cc}}{2}P^cP^c+\frac{\lambda_{ac}}{2}P^aP^c \quad (6)$$

gives the zero-field equilibrium value of the polarization,

$$P^b=\frac{\alpha}{\lambda_{yy}}\rho_2\rho_2'\sin(\varphi_2-\varphi_2')\approx\frac{\alpha}{\lambda_{yy}}\left[\frac{\sqrt{b_3}}{a_3}\frac{a_{20}a_{20}'}{b_2b_2'}\left(\frac{\sigma a_{20}'}{b_2'}+\frac{a_{20}}{\sigma b_2}\right)\right]^{1/2}\sqrt{T_F-T}, \quad (7)$$

which varies critically at T_F as a proper ferroelectric transition.[13,19] Therefore, the dielectric permittivity χ_{Eb}^b follows a standard Curie-Weiss-like behavior, as reported in NFS.[9]

A decrease of the polarization is observed under application of a magnetic field along $\vec{b}\times\vec{c}$. Above a critical field B_{th} the polarization P^b cancels and a component P^c appears.[9] This polarization flop can be interpreted as a first-order transition to phase III, the $m_{ac}1'$ symmetry of which reduces to m_{ac}' under application of the field, canceling P^b and inducing a polarization in the $\vec{a}$-$\vec{c}$ plane. Only the P^c component was reported in NSF.[9] At zero magnetic field the coupling free-energy reads:

TABLE II. Zero-field magnetic point groups (PG), spontaneous polarization $\vec{P}_0$, magnetization $\vec{M}_0$ and toroidal moment $\vec{T}_0$ in phases II, II$'$, and III. Under small electric and magnetic fields one has: $\vec{T}=\vec{T}_0+\hat{\kappa}_E\vec{E}+\hat{\kappa}_M\vec{B}$, $\vec{P}=\vec{P}_0+\hat{\chi}_E\vec{E}+\hat{\alpha}_{EM}\vec{B}$ and $\vec{M}=\vec{M}_0+\hat{\alpha}_{ME}\vec{E}+\hat{\chi}_M\vec{B}$, where $\hat{\kappa}_E=\hat{\alpha}_{EM}=\hat{\alpha}_{ME}=\vec{T}_0=\vec{M}_0=0$ in all the phases of the model. Dielectric $\hat{\chi}_E$, magnetic $\hat{\chi}_M$, and magnetotoroidal $\hat{\kappa}_M$ susceptibilities.

Phases	II	II$'$	III
PG	$2/m1'$	$21'$	$m1'$
$\vec{P}_0,\vec{M}_0,\vec{T}_0$	$\vec{0},\vec{0},\vec{0}$	$P^b,\vec{0},\vec{0}$	$P^aP^c,\vec{0},\vec{0}$
$\hat{\chi}_E,\hat{\chi}_M$	$\begin{pmatrix}\chi_a^a & 0 & \chi_a^c\\ 0 & \chi_b^b & 0\\ \chi_c^a & 0 & \chi_c^c\end{pmatrix}$	$\begin{pmatrix}\chi_a^a & 0 & \chi_a^c\\ 0 & \chi_b^b & 0\\ \chi_c^a & 0 & \chi_c^c\end{pmatrix}$	$\begin{pmatrix}\chi_a^a & 0 & \chi_a^c\\ 0 & \chi_b^b & 0\\ \chi_c^a & 0 & \chi_c^c\end{pmatrix}$
$\hat{\kappa}_M$	$\begin{pmatrix}0 & 0 & 0\\ 0 & 0 & 0\\ 0 & 0 & 0\end{pmatrix}$	$\begin{pmatrix}\kappa_a^a & 0 & \kappa_c^a\\ 0 & \kappa_b^b & 0\\ \kappa_a^c & 0 & \kappa_c^c\end{pmatrix}$	$\begin{pmatrix}0 & \kappa_a^b & 0\\ \kappa_b^a & 0 & \kappa_b^c\\ 0 & \kappa_c^b & 0\end{pmatrix}$

$$F_C=-\chi\vec{P}\,.\,\vec{E}+\frac{\lambda_{aa}}{2}(P^a)^2+\frac{\lambda_{bb}}{2}(P^b)^2+\frac{\lambda_{cc}}{2}(P^c)^2+\frac{\lambda_{ac}}{2}P^aP^c+\beta_cKP^c+\beta_aKP^a+\gamma KJP^b+\mu JP^aP^b+\nu JP^cP^b \quad (8)$$

where $K=\rho_1\rho_2\sin(\varphi_1-\varphi_2)$ and $J=\rho_1\rho_2\cos(\varphi_1-\varphi_2)$. It gives the spontaneous polarization in phase III (in which J=0),

$$P^a=\frac{\lambda_{ac}\beta_c-\lambda_{cc}\beta_a}{\lambda_{aa}\lambda_{cc}-\lambda_{ac}^2}K,\qquad P^b=0,\qquad P^c=\frac{\lambda_{ac}\beta_c-\lambda_{cc}\beta_c}{\lambda_{aa}\lambda_{cc}-\lambda_{ac}^2}K, \quad (9)$$

Equation (9) shows that phase III exhibits spontaneous polarization in the $\vec{a}$-$\vec{c}$ plane. At variance with P^b in phase II$'$, P^c in phase III is induced by the coupling of two order-parameters spanning distinct representations ($\Gamma^+\times\Gamma^-$). Along the thermodynamic path denoted by $\mathcal{P}$ in Fig. 3 the temperature dependence of K is given by

$$K=\rho_1\rho_2=\left\{\frac{a_{10}}{a_3^3}(a_{10}b_2-a_{20}c)\right\}^{1/2}\sqrt{T_{III}-T}, \quad (10)$$

where T_{III} is the critical temperature, at which phase III would take place at zero magnetic field. $a_1=a_{10}(T_{III}-T)+\sigma c$ and $a_2=a_{20}(T_{III}-T)+\sigma b_2$, where a_{10}, a_{20}, and σ are temperature-independent parameters.

The observed property of P^b and P^c to cancel at almost the same critical field[9] is the most remarkable feature of the flop transition. It suggests the existence of a narrow region of stability of the paraelectric phase II *between* phases II$'$ and III. However, it is experimentally unclear in NSF (Ref. 9) if the transition to the high-field phase is a direct (II$'\rightarrow$III)

weakly first-order transition or a sequence (II′ → II → III) of two second-order transitions.

IV. TOROIDIC EFFECTS

A. Macroscopic properties

Applying electric or magnetic fields induces a toroidal moment,

$$\vec{T} = \vec{T}_0 + \hat{\kappa}_E \vec{E} + \hat{\kappa}_M \vec{B}, \tag{11}$$

where $\hat{\kappa}_E$ and $\hat{\kappa}_M$ are the *electrotoroidal* and *magnetotoroidal* susceptibilities. Their nonzero components are summarized for each phase in Table II. Since phases II and II′ are macroscopically invariant under time reversal, one has $\vec{T}_0 = 0$ and $\hat{\kappa}_E = 0$. In phase II, due to space inversion $\hat{\kappa}_M = 0$, whereas in phase II′ the nonzero components of $\hat{\kappa}_M$ are controlled by the toroidal free energy,

$$F_2^T = \rho_2 \rho_2' \sin(\varphi_2 - \varphi_2')(\alpha_{aa} T^a B^a + \alpha_{bb} T^b B^b + \alpha_{cc} T^c B^c + \alpha_{ac} T^a B^c + \alpha_{ca} T^c B^a) + \frac{1}{2} g_{aa} (T^a)^2 + \frac{1}{2} g_{bb} (T^b)^2 + \frac{1}{2} g_{cc} (T^c)^2 + g_{ac} T^a T^c, \tag{12}$$

where α_{ij} and g_{ij} are temperature-independent phenomenological coefficients. Minimizing F_2^T with respect to T^a, T^b, and T^c gives

$$\hat{\kappa}_M^{\mathrm{II}'} = \frac{\rho_2 \rho_2' \sin(\varphi_2 - \varphi_2')}{\Delta} \begin{bmatrix} g_{ac}\alpha_{ca} - g_{cc}\alpha_{aa} & 0 & g_{ac}\alpha_{cc} - g_{cc}\alpha_{ac} \\ 0 & -\frac{\alpha_{bb}}{g_{bb}}\Delta & 0 \\ g_{ac}\alpha_{aa} - g_{aa}\alpha_{ca} & 0 & g_{ac}\alpha_{ac} - g_{cc}\alpha_{aa} \end{bmatrix}, \tag{13}$$

where $\Delta = g_{aa} g_{cc} - g_{ac}^2$. It shows that in the vicinity of T_F the $\hat{\kappa}_M^{\mathrm{II}'}$ components display the same temperature dependence as P^b Eq. (7) varying critically as $\sqrt{T_F - T}$.

In phases III, IV, and V the magnetotoroidal coupling reads

$$F_{\mathrm{coupl}} = (\alpha_{ab} T^a B^b + \alpha_{ba} T^b B^a + \alpha_{cb} T^c B^b + \alpha_{bc} T^b B^c) K + (\alpha_{aa} T^a B^a + \alpha_{ac} T^a B^c + \alpha_{ca} T^c B^a + \alpha_{cc} T^c B^c + \alpha_{bb} T^b B^b) K \,.\, J, \tag{14}$$

where K and J are given below Eq. (8). It yields the susceptibility:

$$\hat{\kappa}_M = \frac{K}{\Delta} \begin{pmatrix} 0 & g_{ac}\alpha_{cb} - g_{cc}\alpha_{ab} & 0 \\ -\alpha_{ba}\Delta/g_{bb} & 0 & -\alpha_{bc}\Delta/g_{bb} \\ 0 & g_{ac}\alpha_{ab} - g_{aa}\alpha_{cb} & 0 \end{pmatrix} + \frac{K \,.\, J}{\Delta} \begin{pmatrix} g_{ac}\alpha_{ca} - g_{cc}\alpha_{aa} & 0 & g_{acz}\alpha_{cc} - g_{cc}\alpha_{ac} \\ 0 & -\alpha_{bb}\Delta/g_{bb} & 0 \\ g_{ac}\alpha_{aa} - g_{aa}\alpha_{ca} & 0 & g_{ac}\alpha_{ac} - g_{aa}\alpha_{cc} \end{pmatrix} \tag{15}$$

Setting J=0 and $\varphi_1 - \varphi_2 = \pi/2$ in Eq. (15) provides the magnetotoroidal susceptibility in phase III,

$$\hat{\kappa}_M^{\mathrm{III}} = \frac{K}{\Delta} \begin{pmatrix} 0 & g_{ac}\alpha_{cb} - g_{cc}\alpha_{ab} & 0 \\ -\alpha_{ba}\Delta/g_{bb} & 0 & -\alpha_{bc}\Delta/g_{bb} \\ 0 & g_{ac}\alpha_{ab} - g_{aa}\alpha_{cb} & 0 \end{pmatrix}, \tag{16}$$

It shows again that the components of $\hat{\kappa}_M^{\mathrm{III}}$ vary with temperature as the P^c polarization in phase III, i.e., as $K = \rho_1 \rho_2$ given by Eq. (10). Thus, in phases II′ and III the magnetotoroidal susceptibility components display the same critical behavior as the corresponding polarization components, i.e., *at constant magnetic field the toroidal moment varies critically as the polarization* $\vec{P}$ at zero field. Figure 6 shows the field dependence of the susceptibility. The scaling of $\vec{T}$ with $\vec{P}$ reflects the inherently magnetoelectric nature of the ferrotoroidic state. Therefore, in phase II′ $\vec{T}$ starts from zero at zero field, increases linearly at low field (except close to $T = T_F$), before reaching a maximum, then decreases and vanishes continuously at a threshold field B_{th}.

From the susceptibilities $\kappa_M^{\mathrm{II}'}$ [Eq. (14)] and κ_M^{III} [Eq. (16)] one can deduce the interplay between the ferroelectric (FE) and ferrotoroidic (FTO) domains under applied magnetic fields in the ferroelectric phases of NFS. The $2_b 1'$ symmetry of phase II′ at zero field displays two FE domains. A B^b field reduces the symmetry to 2_b, inducing a small magnetization M^b and a toroidal moment $T^b = -\alpha_{bb}/g_{bb} B^b \rho_2 \rho_2' \sin(\varphi_2 - \varphi_2')$ with reversed signs in the two domains. Applying a field normal to $\vec{b}$ lowers the symmetry to $2_b'$, preserving the FE domains and inducing a weak magnetization (M^a, M^c) and a toroidal moment (T^a, T^c) normal to $\vec{b}$ but not parallel to the field, with, again, reversed signs in the two domains. The m_{ac}' symmetry of phase III under B^{ac} exhibits also two domains with reversed polarizations and toroidal moments. In each domain the polarization and the toroidal moment are not necessarily parallel.

The domain pattern under applied magnetic field of phase IV, which has the triclinic nonpolar symmetry $\bar{1}1'$ (Fig. 4), presents some remarkable features which deserve to be emphasized despite the fact that this phase is not observed in

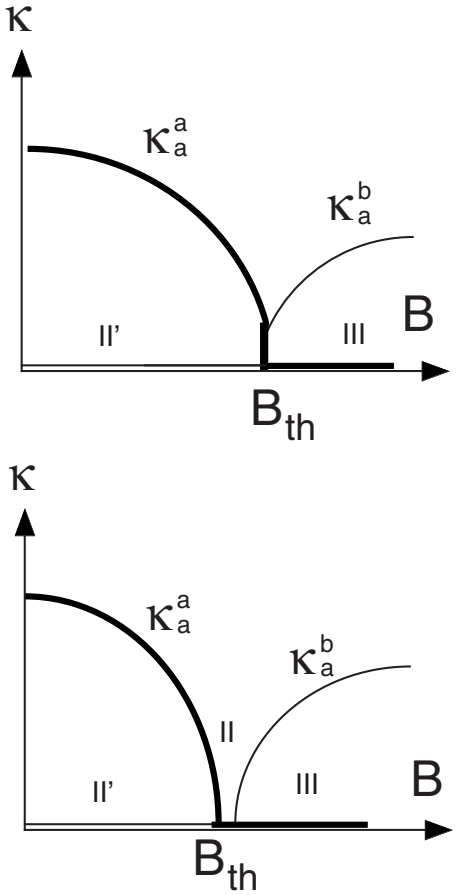

FIG. 6. Field dependence of the magetotoroidal susceptibility. (a) When the II′-III transition is first order. (b) When there is a sequence, II′-II-III, of second-order transitions.

NFS. At zero field its two antiferromagnetic domains cannot be distinguished on using macroscopic vectors. Applying a magnetic field along $\vec{c}$ induces a toroidal moment in the $\vec{a}$-$\vec{c}$ plane (see Table II) and a magnetization parallel to $\vec{b}$. The number of domains is unaffected, but the domains can be distinguished by the orientation $\pm\vec{T}$ of their toroidal moments, while the magnetization is identical in the two domains. Applying a magnetic field perpendicular to $\vec{b}$ induces a toroidal moment parallel to $\vec{b}$, and a magnetization normal to $\vec{b}$. The magnetic domains are unaffected by the field, but can be distinguished by the orientation $\pm\vec{T}$ of their toroidal moments. Applying a field oriented arbitrarily with respect to $\vec{b}$ gives rise to a magnetization and a toroidal moment having both three independent components, in such a way that the three vectors $\vec{B}$, $\vec{T}$, and $\vec{M}$ are neither parallel nor perpendicular. Consequently, a single domain corresponding to a preferred toroidal orientation is favored by the field, which varies with the orientation of the field.

B. Microscopic description

To gain insight into the nature of the microscopic states giving rise to the toroidal moment, one can express the transition order parameter in function of the spins localized at the magnetic atomic positions, instead of the continuous magnetic waves used in the previous sections. In order to visualize the structures, we consider the commensurate approximants of the incommensurate structures of NFS obtained for $\vec{k}=\vec{b}^*$. Note that they do not coincide exactly with the lock-in limit-phases stabilized when $\vec{k}=\vec{b}^*$, which are described in the Appendix. Indeed, additional symmetry breakdowns would take place at the lock-in transitions if the wave vector reaches the value $\vec{k}=\vec{b}^*$.

Denoting by $\vec{s}_1$-to-$\vec{s}_4$ the spins of the four Fe atoms in Fig. 1, with $\vec{s}_i=s_i^a\vec{a}+s_i^b\vec{b}+s_i^c\vec{c}$ $(i=1-4)$, the transition order parameters can be expressed as combinations of spin components. Such an atomic description allows a more refined analysis of the magnetic behavior of NFS, as it involves additional (noncritical) magnetic degrees of freedom described by the four spin waves,

$$\vec{L}_1=\vec{s}_1+\vec{s}_2-\vec{s}_3-\vec{s}_4,\quad \vec{L}_2=\vec{s}_1-\vec{s}_2-\vec{s}_3+\vec{s}_4,$$
$$\vec{N}=\vec{s}_1+\vec{s}_2+\vec{s}_3+\vec{s}_4,\quad \vec{R}=\vec{s}_1-\vec{s}_2+\vec{s}_3-\vec{s}_4. \quad (17)$$

The critical spin waves $\vec{L}_1$ and $\vec{L}_2$ correspond to the lock-in wave vector $\vec{k}_L=(0,1,0)$ and verify the conditions $(\vec{s}_1=-\vec{s}_3,\ \vec{s}_2=-\vec{s}_4)$ imposed by the antitranslations conserved in all the ordered phases. One finds the relationships,

$$L_1^a=\rho_2\cos\varphi_2,\quad L_2^a=\rho_2\sin\varphi_2,\quad L_1^c=\rho_2'\cos\varphi_2',$$
$$L_2^c=\rho_2'\sin\varphi_2',\quad L_1^b=\rho_1\cos\varphi_1,\quad L_2^b=\rho_1\sin\varphi_1, \quad (18)$$

which are analog to Eqs. (1) and (2) for discrete spins, confirming that one copy of Γ^+ and two copies of Γ^- are required for describing the degrees of freedom associated with the magnetic atoms in NFS. The additional waves $\vec{N}$ and $\vec{R}$(at $\vec{k}=0$) transform, respectively, as the total spin of the extended cell, and as the toroidal moment $\vec{T}$. The equilibrium conditions for the order parameters at zero field provide the spin state in the approximant structures,

$$\vec{s}_1=\vec{s}_2\perp\vec{b}(\text{phase II}),\quad \vec{s}_1,\vec{s}_2\perp\vec{b}(\text{phase II}'),$$
$$s_1^a=s_2^a, s_1^c=s_2^c,\quad s_1^b=-s_2^b(\text{phase III}). \quad (19)$$

Figure 7 shows the magnetic structures of phases II, II′ and III satisfying the preceding relationships.

In the approximant of II′ at zero field the spin configuration is given by

$$\vec{s}_1^{(0)}=\frac{1}{4}\begin{pmatrix}\rho_2\cos\varphi_2+\rho_2\sin\varphi_2\\0\\\rho_2'\cos\varphi_2'+\rho_2'\sin\varphi_2'\end{pmatrix},$$
$$\vec{s}_2^{(0)}=\frac{1}{4}\begin{pmatrix}-\rho_2\cos\varphi_2+\rho_2\sin\varphi_2\\0\\-\rho_2'\cos\varphi_2'+\rho_2'\sin\varphi_2'\end{pmatrix},$$

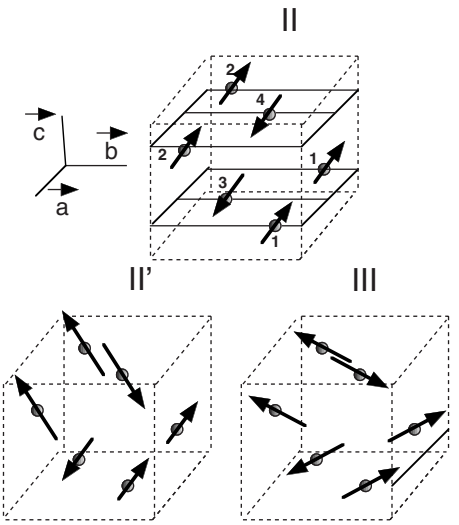

FIG. 7. Calculated orientations of the Fe spins in the monoclinic unit cells of phases II, II′, and III at zero field.

$$\vec{s}_3^{(0)} = -\frac{1}{4}\begin{pmatrix} \rho_2 \cos\varphi_2 + \rho_2 \sin\varphi_2 \\ 0 \\ \rho_2' \cos\varphi_2' + \rho_2' \sin\varphi_2' \end{pmatrix},$$

$$\vec{s}_4^{(0)} = -\frac{1}{4}\begin{pmatrix} \rho_2 \cos\varphi_2 + \rho_2 \sin\varphi_2 \\ 0 \\ \rho_2' \cos\varphi_2' + \rho_2' \sin\varphi_2' \end{pmatrix}. \quad (20)$$

Canceling $\vec{L}_1$, $\vec{L}_2$, and $\vec{N}$ in Eq. (17) provides the "elementary" toroidal spin configuration,

$$\vec{s}_1 = \vec{s}_3 = -\vec{s}_2 = -\vec{s}_4 = \vec{R}/4 \quad (21)$$

represented in Fig. 8(a). Equation (21) gives the spins for a hypothetical "primary ferrotoroidal transition," in which $\vec{R}$ would be the critical order parameter. However it constitutes only part of the actual spin configurations in NFS since $\vec{R}$ *is not* the primary transition order parameter in phase II′, but only a field-induced secondary order parameter. Note that for the axially symmetric phase II′ all the spins in the "elementary configuration" are parallel to $\vec{b}$ [Fig. 8(b)].

Let us analyze the spin configurations arising under magnetic field. In phase II′ at zero field, $\vec{N}=\vec{R}=0$. Under a small applied magnetic field $\vec{B}$, the four vectors $\vec{L}_1$, $\vec{L}_2$, $\vec{N}$, and $\vec{R}$ get contributions proportional to $\vec{B}$,

$$\vec{N} = \hat{\chi}_N\vec{B}, \vec{R} = \hat{\chi}_R\vec{B}, \quad \vec{L}_1 = \begin{pmatrix} \rho_2 \cos\varphi_2 \\ 0 \\ \rho_2' \cos\varphi_2' \end{pmatrix} + \hat{\chi}_1\vec{B},$$

$$\vec{L}_2 = \begin{pmatrix} \rho_2 \sin\varphi_2 \\ 0 \\ \rho_2' \sin\varphi_2' \end{pmatrix} + \hat{\chi}_2\vec{B}, \quad (22)$$

where the matrices of the susceptibilities $\hat{\chi}_N$, $\hat{\chi}_R$, $\hat{\chi}_1$, and $\hat{\chi}_2$ have the same form with $\hat{\chi}_z^y=\hat{\chi}_y^z=\hat{\chi}_y^x=\hat{\chi}_x^y=0$. Applying the field along $\vec{b}$ yields the spins,

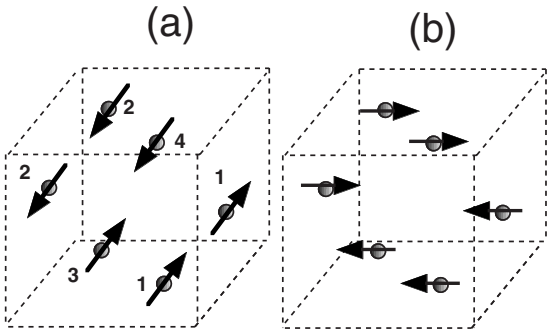

FIG. 8. Orientations of the Fe spins giving rise to a nonzero toroidal moment, deduced from Eqs. (17) and (21): (a) when no additional restriction is put on the symmetry; (b) when the symmetry groups keeps a twofold axis parallel to $\vec{b}$.

$$\vec{s}_1 = \vec{s}_1^{(0)} + \frac{\chi_{Ny}^y + \chi_{Ry}^y + \chi_{1y}^y + \chi_{2y}^y}{4}\begin{pmatrix} 0 \\ B \\ 0 \end{pmatrix},$$

$$\vec{s}_2 = \vec{s}_2^{(0)} + \frac{\chi_{Ny}^y - \chi_{Ry}^y + \chi_{1y}^y - \chi_{2y}^y}{4}\begin{pmatrix} 0 \\ B \\ 0 \end{pmatrix},$$

$$\vec{s}_3 = \vec{s}_3^{(0)} + \frac{\chi_{Ny}^y + \chi_{Ry}^y - \chi_{1y}^y - \chi_{2y}^y}{4}\begin{pmatrix} 0 \\ B \\ 0 \end{pmatrix},$$

$$\vec{s}_4 = \vec{s}_4^{(0)} + \frac{\chi_{Ny}^y - \chi_{Ry}^y - \chi_{1y}^y + \chi_{2y}^y}{4}\begin{pmatrix} 0 \\ B \\ 0 \end{pmatrix}. \quad (23)$$

Similarly, applying the field in the $\vec{a}$-$\vec{c}$ plane yields,

$$\vec{s}_1 = \vec{s}_1^{(0)} + \frac{1}{4} \times \begin{pmatrix} (\chi_{Nx}^x + \chi_{Rx}^x + \chi_{1x}^x + \chi_{2x}^x)B^x + (\chi_{Nz}^x + \chi_{Rz}^x + \chi_{1z}^x + \chi_{2z}^x)B^z \\ 0 \\ (\chi_{Nx}^z + \chi_{Rx}^z + \chi_{1x}^z + \chi_{2x}^z)B^x + (\chi_{Nz}^z + \chi_{Rz}^z + \chi_{1z}^z + \chi_{2z}^z)B^z \end{pmatrix},$$

$$\vec{s}_2 = \vec{s}_2^{(0)} + \frac{1}{4} \times \begin{pmatrix} (\chi_{Nx}^x - \chi_{Rx}^x + \chi_{1x}^x - \chi_{2x}^x)B^x + (\chi_{Nz}^x - \chi_{Rz}^x + \chi_{1z}^x - \chi_{2z}^x)B^z \\ 0 \\ (\chi_{Nx}^z - \chi_{Rx}^z + \chi_{1x}^z - \chi_{2x}^z)B^x + (\chi_{Nz}^z - \chi_{Rz}^z + \chi_{1z}^z - \chi_{2z}^z)B^z \end{pmatrix},$$

$$\vec{s}_3 = \vec{s}_3^{(0)} + \frac{1}{4} \times \begin{pmatrix} (\chi_{Nx}^x + \chi_{Rx}^x - \chi_{1x}^x - \chi_{2x}^x)B^x + (\chi_{Nz}^x + \chi_{Rz}^x - \chi_{1z}^x - \chi_{2z}^x)B^z \\ 0 \\ (\chi_{Nx}^z + \chi_{Rx}^z - \chi_{1x}^z - \chi_{2x}^z)B^x + (\chi_{Nz}^z + \chi_{Rz}^z - \chi_{1z}^z - \chi_{2z}^z)B^z \end{pmatrix},$$

$$\vec{s}_4 = \vec{s}_4^{(0)} + \frac{1}{4} \times \begin{pmatrix} (\chi^x_{Nx} - \chi^x_{Rx} - \chi^x_{1x} + \chi^x_{2x})B^x + (\chi^x_{Nz} - \chi^x_{Rz} - \chi^x_{1z} + \chi^x_{2z})B^z \\ 0 \\ (\chi^z_{Nx} - \chi^z_{Rx} - \chi^z_{1x} + \chi^z_{2x})B^x + (\chi^z_{Nz} - \chi^z_{Rz} - \chi^z_{1z} + \chi^z_{2z})B^z \end{pmatrix}. \quad (24)$$

A microscopic analysis of the magnetic and toroidal effects can be performed by using the effective Hamiltonian corresponding to a second-degree expansion with fixed spin moduli, expressed in function of the spin variables,

$$H^0_{\text{eff}} = \frac{a_{ij}}{2} N^i N^j + \frac{b_{ij}}{2} R^i R^j + \frac{c_{ij}}{2} L^i_1 L^j_1 + \frac{d_{ij}}{2} L^i_2 L^j_2 + e_{ij} N^i B^j, \quad (25)$$

where $\{i,j\}$ run over $\{a,b,c\}$, and the matrices (a,b,c,d,e) verify the monoclinic conditions $(c_{ab}=c_{ba}=c_{cb}=c_{bc}=0)$. H^0_{eff} can be obtained from the Hamiltonian by assuming that the periodicity of the spin configuration is determined by the wave vector $\vec{k}_L=(0,1,0)$. Only the spins belonging to the extended low-symmetry unit-cell appear explicitly in H_{eff} because only the spin degrees of freedom having nonzero values in the ordered phases, corresponding to the wave vectors $\vec{k}_L$ and $\vec{k}=0$, are taken into account. The spin values under applied field are identical in all extended cells. Besides, interactions between distinct extended cells are implicitly present in the effective Hamiltonian, since the four waves $\vec{L}_1$, $\vec{L}_2$, $\vec{R}$, and $\vec{N}$ in Eq. (17) represent sums over all the spins of the crystal, when the crystal periodicity is taken into account, i.e., for general incommensurate wave vectors all the spins would appear in the definition of the preceding waves. Thus, "self-interaction" terms of the $\vec{s}_1$. $\vec{s}_1$ type are present in the effective Hamiltonian. They result from the interaction of one spin in the first extended cell, say $\vec{s}_1$, with a spin located at the same atomic position in a neighboring extended cell.

At the classical level the ground state is determined by minimizing H^0_{eff} with respect to the directions of the spins $\vec{s}_i$. Such an analysis yields the results previously obtained in our macroscopic approach (Sec. IV A). In addition, the equilibrium values of $\vec{N}$ and $\vec{R}$ provide an interesting insight into the properties of the macroscopic magnetization $\vec{M}$ and of the macroscopic toroidal moment $\vec{T}$ because they have the same symmetry, and thus the same qualitative macroscopic behaviors. However, they should not be confused with them. Indeed, the classical fields $\vec{M}$ and $\vec{T}$ are defined with respect to their contributions to the static magnetic field induced by them.[3] If the spins were pointlike localized at the positions of the magnetic atoms, $\vec{M}$ and $\vec{T}$ would identify to $\vec{N}$ and $\vec{R}$, respectively (up to the total volume of the sample).[3] In fact, the actual spin distribution inside the cell is partially delocalized, so that neither the pointlike spins of Eqs. (17) and (20), nor the continuous harmonic magnetic waves description of Eqs. (1) and (2), are sufficient for characterizing all the degrees of freedom contributing to $\vec{M}$ and $\vec{T}$. In particular, in the monoclinic symmetry of NFS $\vec{M}$ and $\vec{T}$ are not even parallel to $\vec{N}$ and $\vec{R}$. Furthermore, in systems with a larger number of atoms in the cell, various spin vectors $\vec{R}_1, \vec{R}_2 \ldots$ transforming as the toroidal moment enter into the spin description, so that the relationship with $\vec{T}$ becomes clearly ambiguous. In principle $\vec{T}$ can even appear when no $\vec{R}$-type vector is permitted in the cell, such unlikely situation requiring, however, a different microscopic mechanism.

In order to find the equilibrium value of $\vec{T}$ vs the spins $\vec{s}_i$, one has to consider its coupling with the basic vectors $\vec{N}$, $\vec{R}$, $\vec{L}_1$, and $\vec{L}_2$. The corresponding effective Hamiltonian reads

$$\begin{aligned} H_{\text{eff}} = H^0_{\text{eff}} &+ \frac{1}{2} g_{ij} T^i T^j + h_{ij} T^i R^j + T^a (B^a \alpha_{ij} L^i_1 L^j_2 + B^c \beta_{ij} L^i_1 L^j_2) \\ &+ T^c (B^a \gamma_{ij} L^i_1 L^j_2 + B^c \delta_{ij} L^i_1 L^j_2) + T^b B^b \varepsilon_{ij} L^i_1 L^j_2 \\ &+ T^a B^b (\varsigma_{ij} L^i_1 L^i_1 + \tau_{ij} L^i_2 L^j_2) + T^c B^b (\upsilon_{ij} L^i_1 L^j_1 + \omega_{ij} L^i_2 L^j_2) \\ &+ T^b (B^a \xi_{ij} L^i_1 L^j_1 + B^c \theta_{ij} L^i_2 L^j_2), \end{aligned} \quad (26)$$

where the matrices (g,h) and $(\delta,\gamma,\alpha,\beta,\varepsilon)$ verify the monoclinic conditions $(c_{ab}=c_{ba}=c_{cb}=c_{bc}=0)$, whereas the matrices $(\varsigma,\tau,\upsilon,\omega,\xi,\zeta,\theta)$ fulfill the conditions $(\omega_{aa}=\omega_{bb}=\omega_{cc}=\omega_{ac}=\omega_{ca}=0)$. Minimizing H_{eff} with respect to the macroscopic variable $\vec{T}$ provides the explicit form of the toroidal moment to the second order in the spin components,

$$\begin{pmatrix} T^a \\ T^c \end{pmatrix} = \frac{1}{\Delta} \begin{pmatrix} -g_{cc} & g_{ac} \\ g_{ac} & -g_{aa} \end{pmatrix} \begin{pmatrix} h_{aa} R^a + h_{ca} R^c + B^a \alpha_{ij} L^i_1 L^j_2 + B^b (\varsigma_{ij} L^i_1 L^j_1 + \tau_{ij} L^i_2 L^j_2) + B^c \beta_{ij} L^i_1 L^j_2 \\ h_{ac} R^a + h_{cc} R^c + B^a \gamma_{ij} L^i_1 L^j_2 + B^b (\upsilon_{ij} L^i_1 L^j_1 + \omega_{ij} L^i_2 L^j_2) + B^c \delta_{ij} L^i_1 L^j_2 \end{pmatrix},$$

$$T^b = -\frac{1}{g_{bb}} (h_{bb} R^b + B^a \xi_{ij} L^i_1 L^j_1 + B^b \varepsilon_{ij} L^i_1 L^j_2 + B^c \theta_{ij} L^i_2 L^j_2), \quad (27)$$

where $\Delta = g_{aa} g_{cc} - g^2_{ac}$. The dependence of $\vec{T}$ on the magnetic spins is different from a simple linear spin combination, even though its equilibrium value results principally from a strong bilinear coupling with the secondary (nonsymmetry-breaking) spin wave $\vec{R}$ under applied field. In particular, Eq. (27) shows that $\vec{T}$ and $\vec{R}$ are not parallel. It also provides the

TABLE III. Lock-in phases induced by the irreducible representations $\Gamma^A,\Gamma^B,\Gamma^C,\Gamma^D$ and their couplings. Magnetic point groups (PGs), magnetic space groups (MSGs), spontaneous values of the polarization $\vec{P}_0$, vector order parameters $\vec{L}_1$ and $\vec{L}_2$. The spontaneous magnetization $\vec{M}$, toroidal moment $\vec{T}$ and their microscopic analogs $\vec{N}$ and $\vec{R}$ vanish in all the phases under zero field.

Phase	A	B	C	D	$A+B$	$A+C$	$A+D$	$B+C$	$B+D$	$C+D$	F
PG	$2/m1'$	$2/m1'$	$2/m1'$	$2/m1'$	$21'$	$m1'$	$\bar{1}1'$	$\bar{1}1'$	$m1'$	$21'$	$1'$
MSG	P_C2/c	P_C2/m'	P_C2'/m	P_C2'/m'	P_C2	P_Cc	$P_S\bar{1}$	$P_S\bar{1}$	P_Cm'	P_C2_1	P_S1
$\vec{P}_0$	$\vec{0}$	$\vec{0}$	$\vec{0}$	$\vec{0}$	P^b	P^aP^c	$\vec{0}$	$\vec{0}$	P^aP^c	P^b	$P^aP^bP^c$
$\vec{L}_1$	L^b	L^aL^c	$\vec{0}$	$\vec{0}$	$L^aL^bL^c$	L^b	L^b	L^aL^c	L^aL^c	$\vec{0}$	$L^aL^bL^c$
$\vec{L}_2$	$\vec{0}$	$\vec{0}$	L^aL^c	L^b	$\vec{0}$	L^aL^c	L^b	L^aL^c	L^b	$L^aL^bL^c$	$L^aL^bL^c$

toroidal susceptibility $\kappa_M^{II'}$, since $\vec{R}$ is linear in $\vec{B}$: $\vec{R}=\hat{\chi}_R\vec{B}$, $\vec{L}_1$, and $\vec{L}_2$ being replaced in Eq. (27) by their zero-field values given in Eq. (18). Note that introducing Eq. (27) into Eq. (26) provides an effective Hamiltonian depending only on the spins, which has the same form as Eq. (25), but with renormalized coefficients.

A detailed identification of the interactions between spins responsible of the onset of a toroidal moment is beyond the scope of the present work as well as the interactions between spins giving rise to the electric polarization $\vec{P}$. Note however that, at variance with the toroidal moment, the electric dipoles depend quadratically and not linearly on the spin variables, due to the invariance of $\vec{P}$ by time inversion.

V. SUMMARY AND CONCLUSION

Our theoretical analysis of the magnetoelectric and toroidic effects in NSF provides an insight into remarkable properties of multiferroic materials: the ferroelectric phase observed in this compound below 6K is induced by two dephased copies of a single order parameter, transforming as the same irreducible representation of the paramagnetic space group. This *symmetry-replication mechanism*, which is disclosed for the first time in multiferroics is allowed because the *effective-continuous* symmetry associated with the phason rotation is broken in incommensurate systems. At the phenomenological level it reflects the property that for incommensurate wave vectors the infinite discrete group of translations has the same effect on the form of the free energy as a continuous group. The close relationship between magnetoelectric and toroidic effects is analyzed in details at the macroscopic and microscopic levels. It shows the inherently magnetoelectric nature of the scaling properties of the ferrotoroidic state. The toroidal moment arising under applied field in antiferromagnetic-ferroelectric structures is induced simultaneously with a spin wave which exhibits the same symmetry properties, but spans different degrees of freedom. More generally, we emphasize the difference between microscopic spins degrees of freedom and the electromagnetic macroscopic magnetization and toroidal fields.

APPENDIX

At $\vec{k}=\vec{b}^*$, Γ^+ splits into the one-dimensional IR's $\Gamma^A+\Gamma^B$, whereas Γ^- splits into $\Gamma^C+\Gamma^D$. L_1^b spans Γ^A; L_1^a and L_1^c span Γ^C; L_2^a and L_2^c span Γ^D, and L_2^b spans Γ^B. This yields an increase in the number of possible stable phases, which are summarized in Table III. One can verify that Phase II has two lock-in phases (denoted C and D in Table III) corresponding to the magnetic space groups P_C2'/m and P_C2'/m'. Phase II′ locks in the phase $C+D$ (P_C2_1) and phase III locks in $B+D$ (P_Cm') and $A+C$ (P_Cc). All the lock-in phases have four Fe atoms in the elementary unit cell of a black-and-white Bravais lattice preserving antitranslations $(\vec{a}\pm\vec{b})/2$.

The spins in the lock-in phases are given by ($\vec{s}_1=-\vec{s}_3$, $\vec{s}_2=-\vec{s}_4$),

$$-A:\ \vec{s}_1=\vec{s}_2\parallel\vec{b},$$

$$-B:\ \vec{s}_1=-\vec{s}_2\parallel\vec{b},$$

$$-C:\ \vec{s}_1=-\vec{s}_2\perp\vec{b},$$

$$-D:\ \vec{s}_1=\vec{s}_2\perp\vec{b},$$

$$-A+B:\ \vec{s}_1,\vec{s}_2\parallel\vec{b},$$

$$-A+C:\ s_1^a=-s_2^a,s_1^c=-s_2^c,s_1^b=s_2^b,$$

$$-A+D:\ \vec{s}_1=\vec{s}_2,$$

$$-B+C:\ \vec{s}_1=-\vec{s}_2,$$

$$-B+D:\ s_1^a=s_2^a,s_1^c=s_2^c,s_1^b=-s_2^b,$$

$$-C+D:\ \vec{s}_1,s_2\perp\vec{b},$$

$$-F\text{:No additional relation.}$$

where F is the phase with minimal symmetry $1'$. Since the phases are commensurate, no symmetry-replication extension of the polymorphism takes place, so that a single copy of each IR is sufficient to yield the full list of ordered phases.

[1] M. Fiebig, J. Phys. D **38**, R123 (2005).
[2] C. Ederer and N. A. Spaldin, Phys. Rev. B **76**, 214404 (2007).
[3] N. A. Spaldin, M. Fiebig, and M. Mostovoy, J. Phys.: Condens. Matter **20**, 434203 (2008).
[4] H. Schmid, J. Phys.: Condens. Matter **20**, 434201 (2008).
[5] V. M. Dubovik and V. V. Tugushev, Phys. Rep. **187**, 145 (1990).
[6] A. A. Gorbatsevich and Y. V. Kopaev, Ferroelectrics **161**, 321 (1994).
[7] D. G. Sannikov and I. S. Zheludov, Sov. Phys. Solid State **27**, 826 (1985).
[8] B. B. Van Aken, J.-P. Rivera, H. Schmid, and M. Fiebig, Nature (London) **449**, 702 (2007).
[9] S. Jodlauk, P. Becker, J. A. Mydosh, D. I. Khomskii, T. Lorenz, S. V. Streltsov, D. C. Hezel, and L. Bohaty, J. Phys.: Condens. Matter **19**, 432201 (2007).
[10] T. Kimura, T. Goto, H. Shintani, K. Ishizaka, T. Arima, and Y. Tokura, Nature (London) **426**, 55 (2003).
[11] K. Taniguchi, N. Abe, T. Takenobu, Y. Iwasa, and T. Arima, Phys. Rev. Lett. **97**, 097203 (2006).
[12] G. Lawes, M. Kenzelmann, N. Rogado, K. H. Kim, G. A. Jorge, R. J. Cava, A. Aharony, O. Entin-Wohlman, A. B. Harris, T. Yildirim, Q. Z. Huang, S. Park, C. Broholm, and A. P. Ramirez, Phys. Rev. Lett. **93**, 247201 (2004).
[13] P. Tolédano, Phys. Rev. B **79**, 094416 (2009).
[14] P. Tolédano, B. Mettout, W. Schranz, and G. Krexner, J. Phys.: Condens. Matter **22**, 065901 (2010).
[15] M. Kenzelmann, A. B. Harris, A. Aharony, O. Entin-Wohlman, T. Yildirim, Q. Huang, S. Park, G. Lawes, C. Broholm, N. Rogado, R. J. Cava, K. H. Kim, G. Jorge, and A. P. Ramirez, Phys. Rev. B **74**, 014429 (2006).
[16] B. Mettout, P. Tolédano, and V. Lorman, Phys. Rev. Lett. **77**, 2284 (1996); B. Mettout and V. Lorman, Symmetry **2**, 15 (2010).
[17] B. Mettout, P. Tolédano, H. Vasseur, and A. M. Figueiredo Neto, Phys. Rev. Lett. **78**, 3483 (1997).
[18] B. Mettout, Phys. Rev. E **74**, 041701 (2006).
[19] J. C. Tolédano and P. Tolédano, *The Landau Theory of Phase Transitions* (World Scientific, Singapore, 1987).
[20] M. Braden (private communication).